Recycling Argon through Metamorphic Reactions: The Record in Symplectites

Lithos 300–301 (2018) 200–211

Contents lists available at ScienceDirect

Lithos

journal homepage: www.elsevier.com/locate/lithos

Recycling argon through metamorphic reactions: The record in symplectites

Christopher S. McDonald [a,*], Daniele Regis [a,b], Clare J. Warren [a], Simon P. Kelley [a], Sarah C. Sherlock [a]

[a] Department of Environment, Earth and Ecosystems, The Open University, Walton Hall, Milton Keynes MK7 6AA, United Kingdom
[b] Geological Survey of Canada, 601 Booth Street, Ottawa, Ontario K1A 0E8, Canada

ARTICLE INFO

Article history:
Received 18 July 2017
Accepted 18 November 2017
Available online 28 November 2017

Keywords:
$^{40}Ar/^{39}Ar$ thermochronology
Phengite
Biotite
Symplectite
Metamorphism

ABSTRACT

The $^{40}Ar/^{39}Ar$ ages of metamorphic micas that crystallized at high temperatures are commonly interpreted as cooling ages, with grains considered to have lost ^{40}Ar via thermally-driven diffusion into the grain boundary network. Recently reported laser-ablation data suggest that the spatial distribution of Ar in metamorphic micas does not always conform to the patterns predicted by diffusion theory and that despite high metamorphic temperatures, argon was not removed efficiently from the local system during metamorphic evolution. In the Western Gneiss Region (WGR), Norway, felsic gneisses preserve microtextural evidence for the breakdown of phengite to biotite and plagioclase symplectites during near isothermal decompression from c. 20–25 to c. 8–12 kbar at ~700 °C. These samples provide an ideal natural laboratory to assess whether the complete replacement of one K-bearing mineral by another at high temperatures completely 'resets' the Ar clock, or whether there is some inheritance of ^{40}Ar in the neocrystallized phase. The timing of the high-temperature portion of the WGR metamorphic cycle has been well constrained in previous studies. However, the timing of cooling following the overprint is still much debated. In-situ laser ablation spot dating in phengite, biotite-plagioclase symplectites and coarser, texturally later biotite yielded $^{40}Ar/^{39}Ar$ ages that span much of the metamorphic cycle. Together these data show that despite residence at temperatures of ~700 °C, Ar is not completely removed by diffusive loss or during metamorphic recrystallization. Instead, Ar released during phengite breakdown appears to be partially reincorporated into the newly crystallizing biotite and plagioclase (or is trapped in fluid inclusions in those phases) within a close system. Our data show that the microtextural and petrographic evolution of the sample being dated provides a critical framework in which local ^{40}Ar recycling can be tracked, thus potentially allowing $^{40}Ar/^{39}Ar$ dates to be linked more accurately to metamorphic history.

1. Introduction

$^{40}Ar/^{39}Ar$ dating is commonly used to constrain the timing and the rate of cooling in high temperature metamorphic terranes via the closure temperature (T_C) formulation suggested by Dodson (1973). This formulation is underpinned by a number of assumptions: (1) that the mineral in question (re)crystallized with an insignificant initial ^{40}Ar concentration; (2) that thermally-activated volume diffusion, observing Fick's 2nd law, redistributed Ar within the mineral after its production, (3) that the grain boundary network surrounding the mineral had a sufficiently low Ar concentration and high connectivity to act as an infinite reservoir (i.e. an 'open' grain boundary system) during the time at which temperatures were high enough for efficient diffusion, and (4) that the grain crystallized at temperatures high enough for diffusion to initially be efficient. Furthermore, the formulation requires a cooling path of 1/T shape.

Many studies document equivocal metamorphic $^{40}Ar/^{39}Ar$ muscovite, phengite (high pressure (HP) muscovite) and biotite ages that are 'too old' to be interpreted as representing the timing of cooling when assessed within a chronological framework defined by higher closure-temperature chronometers such as U—Pb zircon (e.g. Baxter et al., 2002; Li et al., 1994; Warren et al., 2012b). These results are most commonly documented in HP metamorphic terranes, where the temperature was relatively low (< 600 °C), the timescales of metamorphism commonly short (< 10 Ma), and fluid availability and permeability is low, thus limiting the efficiency of diffusion and efficiency of Ar removal from the grain boundary network. There has been much debate about whether the "too old" ages are the result of contamination with 'excess' or 'inherited' ^{40}Ar (decoupled from parent K or inherited from an earlier generation of mineral growth), whether they represent the timing of mineral crystallization, or a combination of the above (e.g. Allaz et al., 2011; Beltrando et al., 2013; de Sigoyer et al., 2000; Di Vincenzo, 2006; Hacker et al., 2003; Li et al., 1999; Putlitz et al., 2005;

* Corresponding author at: School for Earth and Space Exploration, Arizona State University, BOX 876004, Tempe, Arizona 85287-6004, United States.
E-mail address: chris.mcdonald@asu.edu (C.S. McDonald).

https://doi.org/10.1016/j.lithos.2017.11.028

Sherlock and Kelley, 2002; Villa, 1997; Villa et al., 2014; Warren et al., 2011, 2012b). These older ages may also be the result of inefficient diffusive loss from the grain, due to slower diffusion than predicted by laboratory studies, or due to a grain boundary that does not allow argon to escape the grain efficiently. If diffusive loss is more inefficient than current theory suggests then it is much more difficult to link age to temperature, and the Dodson formulation will not provide the correct interpretation.

HP metamorphic mineral assemblages commonly recrystallize to lower pressure assemblages during exhumation. Recrystallization during exhumation has been hypothesized to play a far greater role than diffusion in releasing/remobilizing Ar during metamorphism and deformation, and hence re-setting the $^{40}Ar/^{39}Ar$ 'clock' (Allaz et al., 2011; Kellett et al., 2016; Mulch and Cosca, 2004; Villa, 1997; Villa et al., 2014). The determination of when the target mineral grew during the metamorphic cycle provides a key relative chronological framework for Ar age interpretation, and provides an opportunity to test this hypothesis. This study aims to assess whether the complete replacement of one K-bearing mineral by another at high temperatures completely 'resets' the Ar clock, or whether there is some inheritance of ^{40}Ar in the neocrystallized phase.

The Western Gneiss Region (WGR) of Norway provides the ideal natural laboratory for testing the relative importance of diffusion and recrystallization in resetting the Ar clock during a high temperature metamorphic cycle. The WGR is a ~50,000 km^2 window into the lowest structural levels of the Scandinavian Caledonides, formed during the subduction of Baltica beneath Laurentia during the Caledonian Orogeny (Gee, 1975; Hacker, 2007; Roberts, 2003). Mafic rocks exposed within predominantly amphibolite-facies felsic gneiss preserve localized evidence for recrystallization under eclogite-facies conditions (Bryhni, 1966; Eskola, 1921; Smith, 1984). Coesite (the high pressure polymorph of quartz) has been documented in both mafic and felsic lithologies (e.g. Terry et al., 2000; Wain, 1997; Wain et al., 2000).

The UHP lithologies occur in three separate, antiformal domains which, from south to north, are the Nordfjord-Stadlandet, the Sorøyane, and the Nordøyane domains, together covering an area of 5000 km^2 (Root et al., 2005). This study focuses on the Nordfjord-Stadlandet domain, where the recorded/preserved P–T gradient ranges from the quartz eclogite-facies in the southeast (~23 kbar and ~600 °C) to coesite-stable eclogite-facies in the northwest (~30 kbar and ~700 °C) across 2500 km^2 (Root et al., 2005; Young et al., 2007). Peak conditions were reached between c. 410–400 Ma (Hacker et al., 2010; Kylander-Clark and Hacker, 2014; Root et al., 2004; Young and Kylander-Clark, 2015). Following (near) isothermal decompression from (U)HP conditions, the entire WGR experienced retrograde amphibolite-facies recrystallization at ~700 °C and 10 kbar by c. 399–379 Ma (Spencer et al., 2013; Walsh and Hacker, 2004). According to the results of simple open-system diffusion models, the diffusion of Ar in both white mica and biotite should be efficient at these conditions (Warren et al., 2012a, 2012b).

Published white mica and biotite $^{40}Ar/^{39}Ar$ multi- and single-grain step heating ages from the Outer Nordfjord area range from 389 to 374 Ma and 402–375 Ma, respectively, and interpreted as cooling ages (Berry et al., 1995; Hacker and Gans, 2005; Lux, 1985; Root et al., 2005; Walsh et al., 2007, 2013; Young et al., 2011). More recent single grain fusion and in-situ laser ablation techniques have yielded highly variable white mica $^{40}Ar/^{39}Ar$ ages, both within and between grains in the same sample, as well as between different samples (Warren et al., 2012b). The lack of core-rim profiles indicative of volume diffusion, as well as the inter-grain variability, suggests that a simple model of open-system diffusion does not fit the data and that more than one process may have been responsible for Ar redistribution during the metamorphic cycle.

Phengite in multiple felsic gneiss samples, analyzed using single-grain fusion and in-situ techniques, yielded $^{40}Ar/^{39}Ar$ ages that were significantly older than the timing of peak metamorphism, and, with a range between 507 and 379 Ma, spanned the timing of the whole WGR metamorphic cycle (McDonald et al., 2016; Warren et al., 2012b). $^{40}Ar/^{39}Ar$ ages were heterogeneously distributed both within individual grains and between different grains within the same sample as well as across different samples. These results imply that micas in different lithologies within the WGR lose or gain ^{40}Ar differently during the metamorphic cycle and that the approximations that underpin the Dodson (1973) T_C formulation may not be applicable in this terrane.

The common occurrence of symplectites in felsic gneisses from terranes that have decompressed from pressures >20 kbar at temperatures >650 °C ('diffusion-efficient' conditions) provides an opportunity to test the effects of high-temperature recrystallization on element remobilization (e.g. Heinrich, 1982; Wain et al., 2000; Gilotti and Krogh-Ravna, 2002; Anderson and Moecher, 2007). Of specific interest to metamorphic $^{40}Ar/^{39}Ar$ geochronology is the breakdown of phengite to symplectites of biotite plus plagioclase, which provides an excellent opportunity to assess the transport distances, pathways, sources and sinks of ^{40}Ar in K-rich assemblages as high temperature minerals break down and recrystallize during exhumation.

Garnet-bearing felsic gneisses preserving relict HP metamorphic assemblages are locally preserved in strain shadows around mafic boudins. Different samples preserve different stages of the mineralogical transition from phengite to biotite via symplectization (Wain et al., 2000). The preservation of these symplectites testifies to a lack of deformation during decompression (Hacker et al., 2010), thus allowing the effects of recrystallization at high temperature on Ar removal or redistribution to be investigated. This study focuses on a sample collected from Krokkenakken (Fig. 1), on the northern shore of the Nordfjord, where garnet-bearing gneisses are preserved within the strain shadow of a > 200 m diamter mafic eclogite body.

2. Methods

2.1. Electron microprobe analysis

Major phases were characterized by back-scattered electron images and electron-microprobe analyses of polished thin sections on the Cameca SX100 (5 spectrometer) Electron Microprobe (EMP) at the Open University. Operating conditions were set to 15 kV and 20 nA, with a defocused beam of 10 μm. A ZAF matrix correction routine was applied and a selection of natural standards was used for calibration. Unknowns were bracketed by analyses of internal secondary standards; uncertainty on major element concentrations is <1%. X-ray element maps of Al, Ca, Mg, Si, and Ti in phengite, biotite, and symplectites; and Al, Ca, Fe, Mg, and Si in garnet were obtained from polished thin sections scanned in mosaic mode (4 × 7 grid) with operating conditions of 20 kV and 20 nA. Dwell time was set at 5 ms with a step size of 20 μm. Chemical formulae were calculated stoichiometrically based on 12 oxygens for garnet, 8 for plagioclase, 22 for phengite and biotite, and 23 for amphibole. Representative core-rim analyses of phengite, biotite and plagioclase are shown in Table 1. Full geochemical analyses are provided in Supplementary Table S.1. Minerals abbreviations used in the tables, figures and text are after Whitney and Evans (2010).

2.2. Bulk chemistry determination

Major elements were determined using sample-glass discs prepared by fusing a 5:1 ratio mix of lithium metaborate/tetraborate flux (Spectroflux 105) and powdered samples prepared by jaw crushing and tema mill. Aliquots of ~3 g of sample powder were dried overnight in porcelain crucibles in an over at ~100 °C. 3.59 g of flux and 0.7 g of sample powder were weighted into platinum crucibles and stirred with a glass rod to ensure homogeneity, before being fired in a furnace at 1100 °C for ~20 min. Sample mixtures were stirred every 5 min to remove gas bubbles and promote homogeneity. The melt was poured into a pre-heated brass mold and formed using a sprung press. Discs were left to cool prior to analysis. 1.2 g of sample powder from the dried

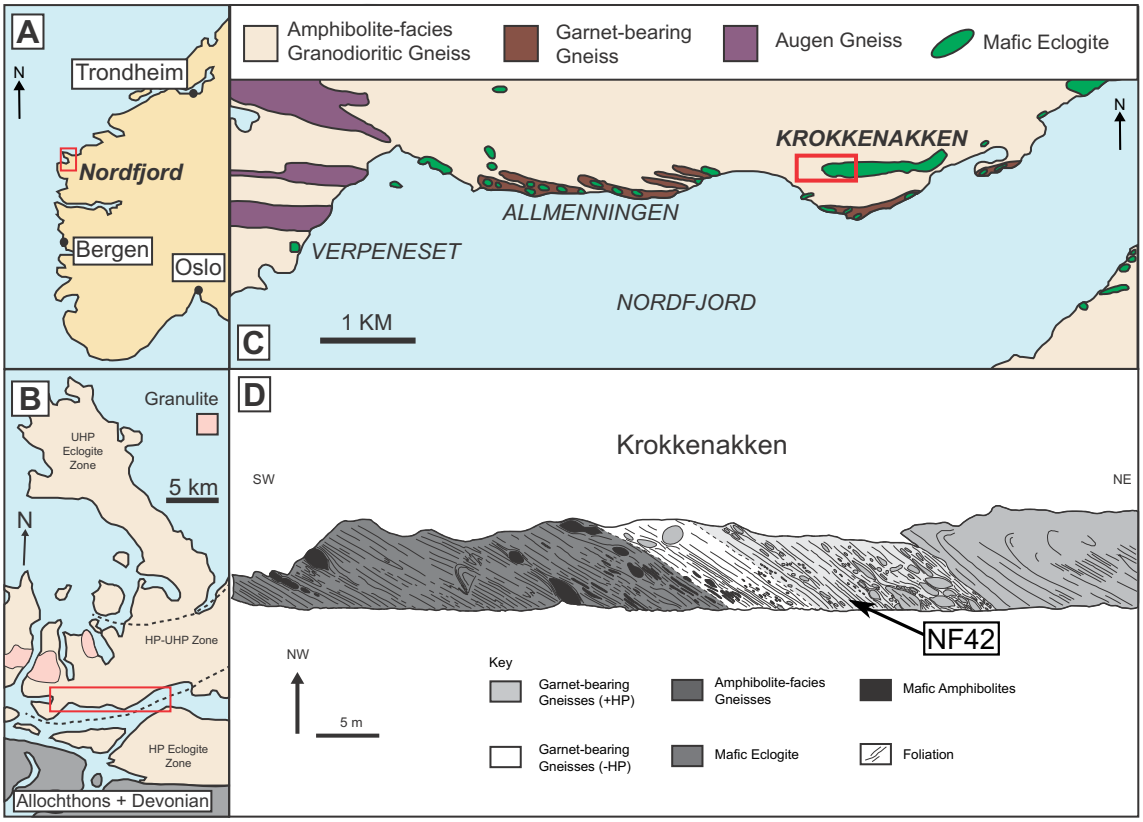

Fig. 1. Simplified geological map of the Nordfjord region. A) location of Nordfjord in western Norway. B and C) location of the Krokkenakken outcrop on the north shore of Nordfjord. D) Field sketch of the Krokkenakken outcrop showing the location of sample NF42. Redrawn from Dransfield (1994).

aliquots was weighed to four decimal places into pre-ignited alumina crucibles. Samples were ignited in the furnace at 1000 °C for 1 h, cooled for 15 min and reweighed to four decimal places. The difference in weight before and after ignition was used to assess the mass loss on ignition for each sample.

Trace elements were determined from pressed sample powder pellets formed by thoroughly mixing approximately 9.5 g of sample powder with 0.9 ml of Polyvinylpyrollidone(PVP)-methyl cellulose binder using the 'bag technique' (Watson, 1996). The mixture was emptied into a hardened steel mold and formed into a pellet using a hydraulic

Table 1
Representative mineral chemistry of phengite, biotite, plagioclase, and amphibole.

Mineral	Phengite		Idioblastic biotite		Symplectic biotite		Plagioclase		Amphibole	
Position	Core	Rim	Core	Rim	Core	Rim	Core	Rim	Core	Rim
SiO_2	49.70	49.80	39.30	37.70	38.00	37.60	65.80	54.30	46.02	46.53
TiO_2	0.20	0.30	2.40	2.10	1.70	2.60	0.00	0.00	0.57	0.52
Al_2O_3	27.30	28.10	15.70	17.60	17.10	16.70	21.60	28.90	13.66	12.74
Cr_2O_3	0.00	0.00	0.00	0.10	0.10	0.10	0.00	0.00	0.04	0.07
FeO	2.00	1.70	10.90	12.80	12.40	13.70	0.10	0.00	9.07	9.24
MnO	0.00	0.00	0.00	0.00	0.00	0.00	0.00	0.00	0.06	0.08
MgO	3.70	3.20	16.40	14.50	16.10	14.60	0.00	0.00	13.93	14.06
CaO	0.00	0.00	0.00	0.00	0.00	0.10	2.40	11.60	11.25	11.49
Na_2O	0.40	0.30	0.10	0.10	0.10	0.10	10.40	5.20	1.23	1.24
K_2O	9.60	9.80	8.80	9.40	9.40	9.50	0.10	0.10	0.77	0.62
Cl	0.10	0.10	0.30	0.10	0.20	0.20	0.00	0.00	0.09	0.05
F	0.00	0.00	0.00	0.00	0.00	0.00	0.00	0.00	0.01	0.00
Total	93.00	93.40	93.90	94.50	95.10	95.10	100.40	100.00	96.69	96.64
Si	6.80	6.70	5.80	5.60	5.60	5.60	2.90	2.50	6.65	6.73
Ti	0.00	0.00	0.30	0.20	0.20	0.30	0.00	0.00	0.06	0.05
Al	4.40	4.50	2.70	3.10	3.00	2.90	1.10	1.50	2.33	2.17
Cr	0.00	0.00	0.00	0.00	0.00	0.00	0.00	0.00	0.00	0.01
Fe	0.20	0.20	1.30	1.60	1.50	1.70	0.00	0.00	1.10	1.12
Mn	0.00	0.00	0.00	0.00	0.00	0.00	0.00	0.00	0.01	0.01
Mg	0.70	0.70	3.60	3.20	3.50	3.20	0.00	0.00	3.00	3.03
Ca	0.00	0.00	0.00	0.00	0.00	0.00	0.10	0.60	1.74	1.78
Na	0.10	0.10	0.00	0.00	0.00	0.00	0.90	0.50	0.34	0.35
K	1.70	1.70	1.70	1.80	1.80	1.80	0.00	0.00	0.14	0.12
Cl	0.00	0.00	0.10	0.00	0.10	0.10	0.00	0.00	0.04	0.02
F	0.00	0.00	0.00	0.00	0.00	0.00	0.00	0.00	0.00	0.00
Total	13.90	13.90	15.60	15.60	15.70	15.70	5.00	5.00	15.42	15.39

press. The sample pellets were dried overnight in the oven at ~100 °C prior to analysis. Results of XRF analyses are presented in Supplementary Material S.2.

2.3. Thermodynamic modelling

Symplectites form from the breakdown of unstable HP phases (e.g. phengite and pyroxene) into two or more minerals at lower P–T conditions. Symplectites provide evidence that textural and compositional equilibrium was attained only on a domainal scale. This lack of textural equilibrium represents a challenge when modelling the metamorphic evolution of the sample. In the present case, a simplified approach was used to constrain the P–T evolution of the major phases:

(i) the whole rock composition, determined by XRF, was used to model the growth of the HP assemblage as well as the symplectites. Microstructural evidence suggests that amphibole, biotite, and plagioclase formed from the breakdown of phengite and pyroxene (most probably omphacite, e.g. Wain et al., 2000). Garnets were replaced by fine grained aggregates of biotite and plagioclase. Following previous work (e.g. Godard and Mabit, 1998; Groppo et al., 2015) we have assumed the whole rock volume was chemically involved and behaving as a closed-system during symplectite formation;
(ii) the retrograde formation of amphibole–plagioclase symplectites was constrained by the plagioclase–hornblende thermobarometer (temperatures using the calibration of Blundy and Holland, 1990; Holland and Blundy, 1994 and pressures using the calibrations of Anderson and Smith, 1995; Schmidt, 1992);
(iii) the reconstructed metamorphic evolution was compared with published P–T paths for the WGR.

The evolution of sample was modelled in the simplified MnNCKFMASTH system using Perple_X (version 6.6.8, Connolly, 1990). The pseudosection was calculated using the internally consistent thermodynamic database (hp04ver.dat) and the equation of state for H_2O of Holland and Powell (1998) and Holland and Powell (2011). Solid solution models include garnet (Holland and Powell, 1998), omphacite (Holland and Powell, 1996), plagioclase (Fuhrman and Lindsley, 1988), phengite (Holland and Powell, 1998), biotite (Tajcmanová et al., 2009), chlorite (Holland et al., 1998), amphibole (Dale et al., 2000), staurolite (Holland and Powell, 1998), chloritoid (White et al., 2000), and melt (Holland and Powell, 2001; White et al., 2001). Additionally, quartz, aluminum silicates, zoisite, lawsonite, titanite, rutile, and ilmenite were included as pure phases.

2.4. Diffusion modelling

In order to determine the expected $^{40}Ar/^{39}Ar$ 'cooling' ages of phengite, biotite and plagioclase for a purely diffusive, open system given the best-fit post-crystallization P-T-t history, diffusion ages were modelled using DiffArg_P, which incorporates the pressure-dependance of Ar diffuion in muscovite (modified from DiffArg after Wheeler, 1996; Warren et al., 2012a). All models were calculated for cylindrical diffusion geometry, with a Crank–Nicholson time integration solver, and a time step of 10 (Wheeler, 1996).

On the basis of petrographic observation constraints, 1 mm radius phengite was modelled as crystallizing at peak pressure conditions of 23.5 kbar and 710 °C. It then decompressed to 12 kbar (at 680 °C) over 12 Ma (calculated from the difference between the youngest published U—Pb zircon, and the weighted average titanite age (Root et al., 2004; Spencer et al., 2013) followed by linear cooling at rates of 10, 25, 50, 70, and 100°CMa^{-1}. Current estimates for the cooling rates of the WGR range from 20 to 90°CMa^{-1} based on the assumption that $^{40}Ar/^{39}Ar$ ages represent cooling through the muscovite closure temperature of ~450 °C (Hacker et al., 2010; Kylander-Clark et al., 2008; Root et al., 2004, 2005; Walsh et al., 2013). Decompression set so that P reached zero at the same time as T.

For modelling purposes, biotite and plagioclase were assumed to have crystallized at conditions of 12 kbar and 680 °C. Cooling initiated immediately in the models and multiple models were run with the same cooling rates as the white mica models. Idioblastic biotite was modelled using a grain radius of 0.5 mm while the symplectic biotite and plagioclase were modelled with a grain radius of 0.25 mm.

To determine the possible affects of variations in the model starting temperatures, pressures, grain sizes, and cooling rates, a sensitivity analysis was performed. Muscovite peak temperatures and pressures were modelled at ±50 °C and ±1.5 kbar, to reflect uncertainties in the modelled peak metamorphic conditions. Amphibolite-facies conditions for muscovite, biotite, and plagioclase were also modelled at ±50 °C and ±5 kbar. Grain size was modelled at 0.25–1.5 mm for each mineral at the above mentioned cooling rates.

Model results and sensitivity analysis (Table 3a, b, and Supplementary Tables S.4) are reported as bulk (area-integrated) age differences between the timing of cooling initiation based upon the U-Pb zircon and titanite ages, and the modelled grain age.

2.5. $^{40}Ar/^{39}Ar$ analysis

Polished thick sections (~250 μm thick; Fig. 2D) were prepared by adhesion to glass slides with cyanoacrylate ("super glue"). Sections were removed from the glass by soaking in acetone for up to 24 h and then cut into 5 × 5 mm squares, washed in acetone or methanol and distilled water, and packed into aluminum foil packets, which were irradiated at McMaster University Reactor, Ontario.

High spatial resolution single spot and traverse analyses on polished thick sections were achieved using a New Wave Systems Nd-YAG 213 nm ultraviolet (UV) laser coupled to a Nu Instruments Noblesse gas mass spectrometer run in single-collector mode. Prior to analysis, samples were loaded into an ultra-high vacuum laser port, warmed under a heat lamp for 8 h to reduce atmospheric background levels and left to pump down for at least 48 h. Analyses consisted of ablating 50/30/15 μm diameter spots for 90 s followed by 90 s gettering time. Active gas species were gettered using two SAES AP10 Zr-Al getters (one at room temperature and the other at 450 °C). Peaks of ^{40}Ar, ^{39}Ar, ^{38}Ar, ^{37}Ar and ^{36}Ar were scanned ten times each and the data extrapolated back to the inlet time (time zero).

Irradiation flux was monitored using the biotite standard GA-1550 with an age of 99.74 ± 0.10 Ma (Renne et al., 2011). Sample *J* values and uncertainties are given in Supplementary Table S.3 and were calculated by linear interpolation between two bracketing standards. The following corrections were applied to the standards: $(^{39}Ar/^{37}Ar)Ca = 0.00065 \pm 0.0000033$, $(^{36}Ar/^{37}Ar)Ca = 0.0002654 \pm 0.0000013$, $(^{40}Ar/^{39}Ar)K = 0.0085 \pm 0.0000425$ based on analyses of Ca and K salts; only the K correction was applied to the analyzed samples due to negligible Ca in the sample micas. Background (blank) measurements bracketed every 1–2 sample measurements. Analyses were corrected for mass spectrometer discrimination using an assumed value of 295, determined from regular analysis of modern glass.

Data were reduced using the in-house software package ArMaDiLo using a decay constant of $5.530 \times 10^{-10} \pm 0.013$ a^{-1} (Renne et al., 2011). Age uncertainties are reported to 2σ; uncertainties on the isotopic measurements are reported to 1σ. The maximum and minimum phengite, biotite, and plagioclase $^{40}Ar/^{39}Ar$ ages are reported in Table 2. The full dataset is provided in Supplementary Table S.3.

3. Results

3.1. Petrography and mineral chemistry

Sample NF42 is a medium-grained, unfoliated and highly symplectized gneiss containing quartz, garnet, biotite, symplectites of

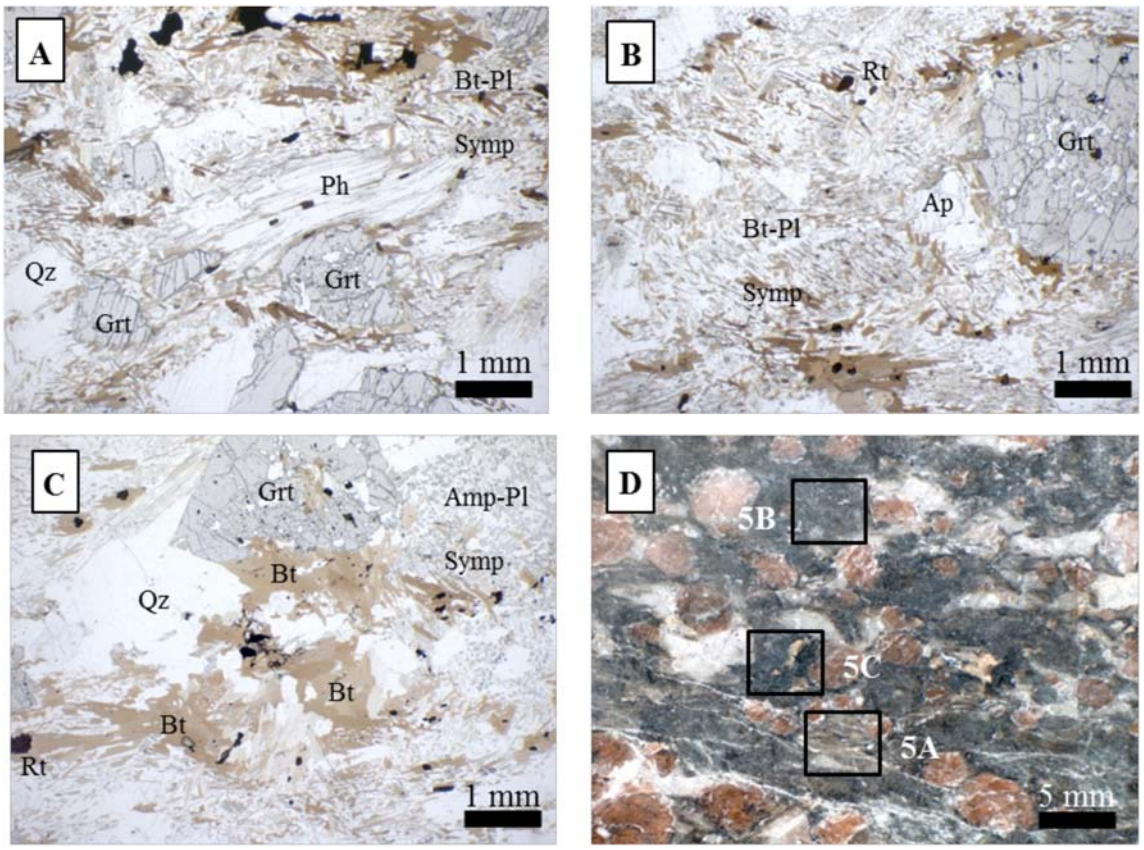

Fig. 2. Photomicrographs of symplectic gneiss; A) large (>2 mm) HP phengite crystals associated with garnet and quartz; B) biotite–plagioclase symplectites replacing phengite; C) idioblastic biotite growing from the biotite–plagioclase symplectite and D) photograph of the polished slab showing the localities of the in-situ analyses in Fig. 5. Mineral abbreviations after Whitney and Evans (2010).

biotite-plagioclase and amphibole-plagioclase, and phengite (Figs. 2 and 3, and Supplementary Material S.5). Accessory phases include kyanite, chlorite, rutile, apatite, and zircon. There is no petrographic evidence for partial melting in this sample (Peterman et al., 2009; Wain et al., 2000).

Phengite relics make up ~5–6% of the sample (Fig. 2A). Grain radii vary from 300 μm to 1100 μm (Fig. 2A, Table 1). Si concentrations range from 6.8 atoms per formula unit in the geographic core to 6.6 at in narrow (<50 μm) rims (Fig. 3A). Grains are commonly replaced at their rims by biotite-plagioclase symplectites.

Biotite crystallizes in two different microstructural, and textural domains: (i) in symplectites pseudomorphing phengite, with the grain size coarsening outwards from core to rim (40–200 μm laths, Fig. 3C), and (ii) randomly oriented aggregates of grains within the matrix (300–1200 μm, Fig. 3B). The biotite–plagioclase symplectites make up approximately ~50 vol% (Fig. 2B). Biotite in the symplectites is Mg-rich with X_{M_g} (Mg/(Mg + Fe) values of 0.65–0.70 and Ti contents ranging from 0.12–0.31 apfu (Table 1). Geochemical analysis and maps (Fig. 3C) show that each grain is homogeneous in geochemistry; and that the variability seen is between individual grains within the symplectite (detailed geochemical maps are supplied Supplementary Material S.5).

Idioblastic biotites form approximately 10 modal% of the sample (Fig. 2C) and are found in the matrix, occasionally adjacent to garnet and quartz, but never adjacent to phengite. They are similar in composition to the symplectitic biotites, with X_{Mg} values of 0.67–0.73 and Ti contents ranging from 0.21–0.32 apfu (Table 1). Geochemical maps show that these grains are relatively homogeneous cores and narrow (<5 μm) rims (Fig. 3D). The idioblastic grains contain inclusions of plagioclase (Fig. 2C), suggesting that they formed by coarsening of the symplectite biotites.

Plagioclase is found within the symplectic domains associated with biotite or amphibole and forms anhedral grains with a typical grain

Table 2
Summary data table of phengite, biotite, and plagioclase in-situ analyses.

				UV *in-situ* ages		
				Oldest age	Youngest age	Wtd Mean age
Sample	Location	Mineral	n#	Ma (±1σ)	Ma (±1σ)	Ma (±1σ)
NF42	Krokkenakken	Phengite	41	517.7 ± 2.8	388.8 ± 2.3	398.1 ± 1.3
		Idioblastic Biotite	25	398.8 ± 3.1	385.6 ± 4.7	392.2 ± 1.1
		Symplectic Biotite	10	391 ± 11	375 ± 20	384.8 ± 2.4
		Symplectic Plagioclase	12	434 ± 42	378 ± 65	392.0 ± 7.5

n# = number of spots
Sample Location 61°54′53.73″ N 005°20′16.49″ E

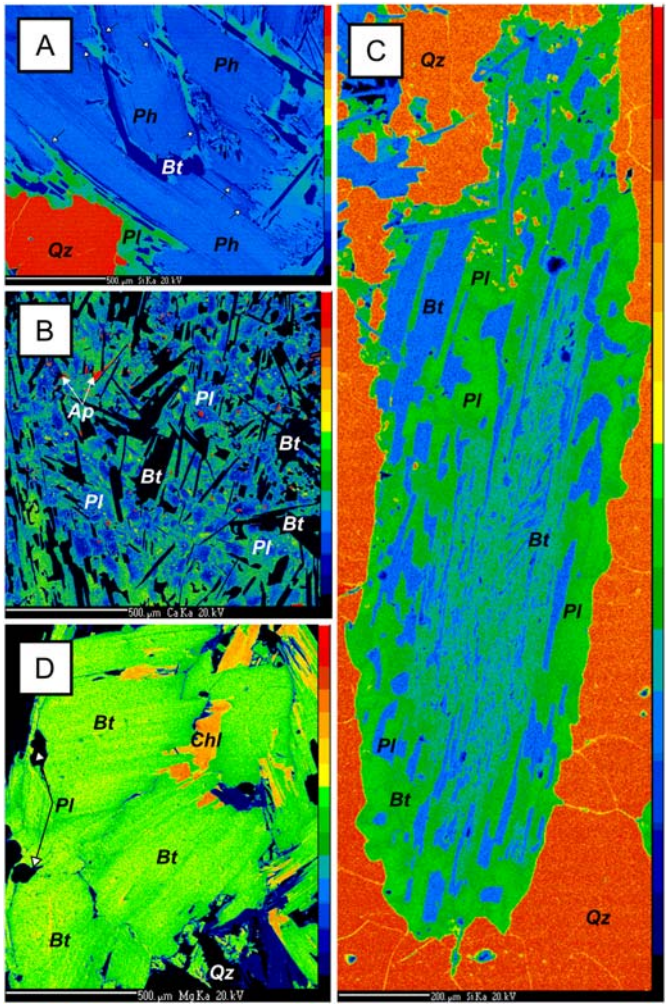

Fig. 3. Microprobe X-ray compositional maps of phengite, symplectitic microtextural domains and biotite. A) Si map showing homogeneous phengite grains (blue). Arrows denote the location of lower Si rims. B) Ca map showing chemically-zoned plagioclase within the randomly orientated symplectite. C) Si map of a symplectite pseudomorph after phengite; orange: quartz, green: plagioclase and blue: biotite. D) Mg map showing homogeneous idioblastic biotite (green) with minor late chlorite (orange). Mineral abbreviations after Whitney and Evans (2011). (For interpretation of the references to colour in this figure legend, the reader is referred to the web version of this article.)

size of 80–140 μm (Fig. 2B). X-ray compositional maps (Fig. 3B) show that the grains are compositionally zoned, with low-Ca cores ($An_{11}Ab_{89}Or_0$) and higher-Ca rims ($An_{45}Ab_{55}Or_0$).

Garnet crystals form 10–15% of the sample, are sub- to anhedral in shape and range from 0.5–15 mm in diameter. Garnets contain abundant, randomly-oriented inclusions of quartz, rutile, white mica, and apatite. Minor replacement of garnet by biotite and plagioclase (Fig. 2A-C) is visible at grain rims. Grains are zoned in X_{Fe} (0.66 in the core to 0.50 in the rim) and X_{Mg} (0.14 in the core to 0.31 at the rim), whilst X_{Ca} is more homogeneous, varying from 0.18 in the core to 0.19 at the rim. Some grains show a high-Ca annulus between the core and rim at X_{Ca}~0.23. X_{Mn} is low throughout garnet at 0.01–0.02 (Supplementary Material S.5).

Fine-grained amphibole is associated with plagioclase in symplectites that form ~10 modal % of the sample. Amphiboles are magnesio-hornblende in composition with $X_{Mg} = 0.68–0.74$ (Table 1).

Rare small kyanite crystals (50–100 μm) are present in the matrix (mostly at the contact with garnet rims) whilst rutile, zircon, and apatite are present in both the matrix and included in garnet (Supplementary Material S.5).

3.2. Pressure-temperature path

The pseudosection in Fig. 4a shows the modelled metamorphic assemblages for the considered bulk composition between 2.5 and 25 kbar and 300–900 °C. The model shows that the compositions of phengite and garnet rim ($Si_{phe} = 3.35–3.37$; $Fe_{grt} = 0.54–0.46$ $Mg_{grt} = 0.26–0.34$ $Ca_{grt} = 0.15–0.22$) overlap in fields where the high-pressure phengite is stable with garnet + omphacite + rutile + quartz ± kyanite ± amphibole between 660 and 760 °C and 22–25 kbar (Fig. 4b).

During decompression from the HP stage, at an approximate T of 700 °C, the pseudosection suggests that feldspar becomes stable at <16 kbar and biotite at <12 kbar. This marks the beginning of symplectite formation; phengite is no longer stable at conditions below 7–11 kbar and <660 °C. The X_{Mg} and X_{Na} compositions of biotite and plagioclase help to constrain the conditions of phengite replacement by biotite-plagioclase symplectites. The modelled isopleths in biotite and plagioclase suggest that the symplectites formed at $T < 720$ °C and $P < 12$ kbar following (near) isothermal decompression from peak pressures (Fig. 4b).

The compositions of amphibole and plagioclase in equilibrium in symplectic domains constrain the PT conditions of replacement of earlier pyroxene. The amphibole-plagioclase thermobarometer (Anderson and Smith, 1995; Blundy and Holland, 1990; Holland and Blundy, 1994; Schmidt, 1992) suggests crystallization at 660 ± 70 °C and 7.9 ± 1.1 kbar.

3.3. Diffusion modelling

Diffusion modelling results are summarized in Table 3a. The model results suggest that in an open, purely diffusive system, 1 mm radius phengite grains should yield bulk ages that are 29.1–13.2 Ma younger than the time at which cooling started (Δt), depending on the cooling rate (10–100°CMa^{-1}). A conservative estimate for the cooling rate of 25°CMa^{-1} suggests Δt = 11.1 Ma. Furthermore, the models suggest that 0.5 mm biotite grains should yield Δt = 12.5 Ma at 25°CMa^{-1}, 32.9 Ma at 10°CMa^{-1} and 2.9 Ma at 100°CMa^{-1}). 0.25 mm biotite grains cooling at 25°CMa^{-1} should yield Δt = 13.4 Ma, and 0.25 mm plagioclase grains should yield Δt = 13.2 Ma (slower and faster cooling at 10–100°CMa^{-1} should yield age differences of 35.0–3.1 and 34.6–3.1 Ma, for 0.25 mm biotite and plagioclase respectively).

3.4. $^{40}Ar/^{39}Ar$ laser spot dating

Forty-one spots on 5 phengite grains yielded ages varying from 517.7 ± 5.6 Ma to 388.8 ± 4.6 Ma (Fig. 5A). Age distributions are patchy, with clusters of 'older' ages in regions that are neither associated spatially with the geographical nor the geochemical cores of the phengite (Fig. 5A). Ten spots on 3 different symplectite biotite grains yielded ages from 488 ± 36 Ma to 329.8 ± 9.2 Ma (Fig. 5 B1, B2). Twelve spots on 12 different symplectite plagioclase grains yielded highly variable $^{40}Ar/^{39}Ar$ ages from 687 ± 264 to 93 ± 1050 Ma (Fig. 5 B1, B2). Three analyses had ^{39}Ar measured/^{39}Ar background measurements <2 (analyses GM7,GM11, and GM12). The calculated ages have large errors, are therefore not considered robust and are ignored for the purposes of further discussion. Ignoring these three analyses, the plagioclase yielded ages ranging from 434 ± 84 Ma to 378 ± 130 Ma. Twenty-six spots on 6 grains of idioblastic biotite yielded a range of ages from 448 ± 5.8 Ma to 376.6 ± 6.4 Ma. There is no systematic distribution of age within the grains (Fig. 5C).

4. Discussion

4.1. Metamorphic evolution

Three main metamorphic stages have been recognized in the Krokkenakken gneisses based on microtextural relationships, crystal chemistry, conventional thermobarometry and pseudosection modelling.

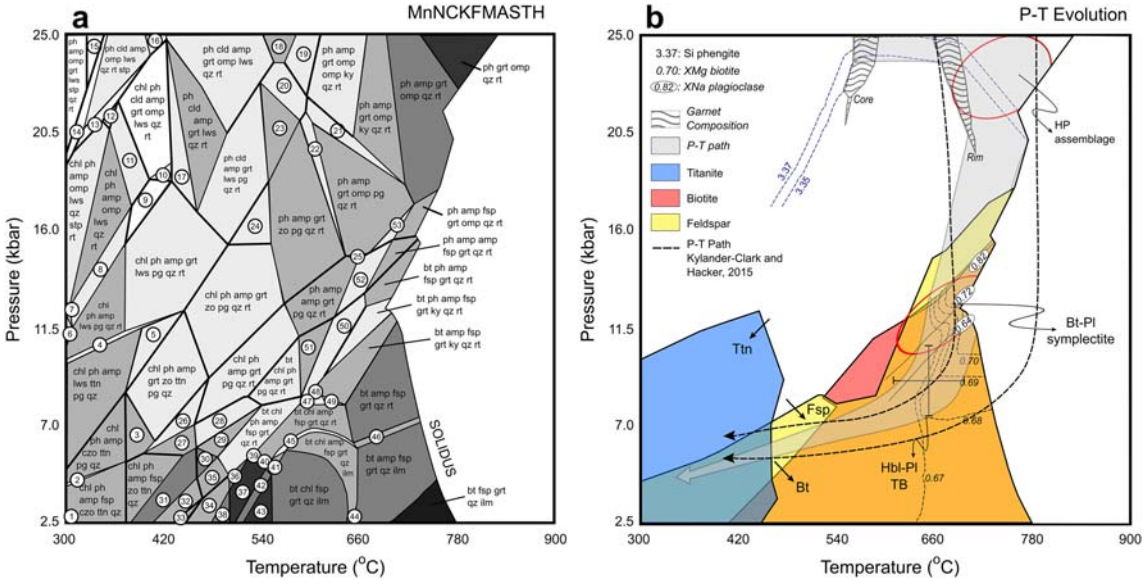

Fig. 4. a) P–T pseudosection constructed for the bulk composition of the sample of symplectic gneiss (in wt% SiO_2: 60.02, TiO_2: 1.12, Al_2O_3: 16.86, FeO: 7.74, MnO: 0.10, MgO: 4.90, CaO, 3.77, Na_2O: 2.19, K_2O: 2.32). Number fields are defined in Supplementary Material S.6. Mineral abbreviations after Whitney and Evans (2011). b) P–T evolution for the symplectic gneiss showing the modelled P–T path experienced by the sample (grey arrow) with the approximate positions of the HP assemblage, the area Bt–Pl symplectite stability, the Hbl—Pl thermobarometry results, the titanite stability field; and biotite-in and plagioclase feldspar-in reactions. The location of the core and rim compositions of garnet is taken from the intersection of the X_{Fe}-, X_{Mg}-, and X_{Ca}-isopleths. P–T path for Nordfjord from Kylander–Clark and Hacker, (2014) shown for comparison.

The first stage occurs under prograde conditions with the growth of garnet. The major element zoning in the garnets core and rim are interpreted as reflecting this prograde growth. Peterman et al. (2009) have also documented prograde-zoned garnet at this locality. Eclogite-facies conditions followed the prograde growth of garnet and are characterized by the assemblage phengite + garnet + omphacite + quartz + rutile ± amphibole ± kyanite. Because of the poor preservation of eclogitic mineral relics such as omphacite, this stage can only be loosely constrained at 20–25 kbar and 670–770 °C (Fig. 4b).The white mica solution model (Holland and Powell, 1998) correctly predicts the stability field of K-rich white micas but does not incorporate the right amount of Na. The main consequence of this is the modelled appearance of paragonite (Pg in Fig. 4a).

Although amphibole, interpreted as part of the HP assemblage, has not been observed in the sample, the model shows that the amount of it stable in these fields corresponds to <2 vol%. Therefore, we cannot exclude that amphibole was part of the high-pressure assemblage and it was subsequently replaced by later phases. Kyanite probably once included in garnet rims later replaced by biotite + plagioclase aggregates (Supplementary Fig. S.5), has been interpreted as part of the same assemblage. The calculated HP conditions overlap with the data presented for the same area (e.g. Cuthbert et al., 2000; Wain, 1997).

Peak pressure conditions were followed by (near)-isothermal decompression to amphibolite-facies conditions of T ~700 °C and $P < 12$ kbar as documented by the growth of biotite-plagioclase and amphibole-plagioclase symplectites developed after phengite and pyroxene respectively. The association of amphibole and plagioclase in fine-grained symplectites has been documented in other HP gneisses from the WGR (e.g. Wain et al., 2000) and has been interpreted as forming from the breakdown of an HP pyroxene (e.g. omphacite). The pseudosection constraints presented here provide similar PT estimates to those previously presented for the WGR gneisses (e.g. Cuthbert et al., 2000; Engvik et al., 2007; Hacker, 2007; Johnson et al., 2007; Labrousse et al., 2004; Root et al., 2005; Terry et al., 2000; Terry and Robinson, 2003; Wain, 1997; Wain et al., 2000; Walsh and Hacker, 2004). These calculated conditions indicate that the amphibole-plagioclase symplectites formed after the biotite-plagioclase symplectites; however, the pseudosection suggests that omphacite is unstable below 15 kbar. Therefore, we suggest that the amphibole-plagioclase symplectites most probably re-equilibrated at lower P–T conditions after formation.

The timing of titanite crystallization plays an important role in the interpretation of the $^{40}Ar/^{39}Ar$ age patterns, as the titanite U—Pb age has been used to constrain the amphibolite-facies recrystallization across the WGR (Krogh et al., 2011; Schärer and Labrousse, 2003; Spencer et al., 2013; Tucker et al., 1987). The conditions of titanite crystallization are controlled primarily by the bulk rock Ca/Al ratio (Frost et al., 2001). In rocks with high Ca/Al ratios, titanite can be stable up to granulite-facies conditions (Frost et al., 2001). However, in orthogneisses, such as those from the WGR, titanite is only stable at much lower P–T conditions (Frost et al., 2001). A large dataset of titanite U—Pb ages from across the WGR accompanied by pseudosections of different titanite-bearing rocks showed both that the ages are widely variable and that titanite is stable across a broad range of PT conditions depending on the bulk composition (Spencer et al., 2013). The titanite stability field in the pseudosection presented here (Fig. 4b) overlaps with the titanite-in reactions published by Spencer et al. (2013) for comparable bulk compositions at $T < 500$ °C and $P < 12$ kbar. Therefore, we suggest that titanite crystallization occurred *syn-* to post-symplectite formation.

4.2. Modelled vs. observed age ranges: Are the "ages" cooling ages?

The diffusion modelling predicts that at cooling rates of 25°CMa^{-1}, the phengite, idioblastic biotite, symplectite biotite and symplectite plagioclase grains should yield Δt of 11.1, 12.5, 13.4, and 13.2 Ma respectively.

The model results are variably sensitive to a number of uncertainties, many of which have previously been discussed in detail (Warren et al., 2012b). Most of the model input parameters affect the whole popuation, and would not generate a spread of ages, rather they would just shift the model age to older or younger values. For example uncertainties in the activation energy (E_a) and the diffusion coefficient (D) lead to an uncertainty of ±4 Ma on the resulting model age.

In the phengite models, varying the starting temperature and pressure by ±50 °C and ±1.5 kbar, respesctively, showed no change in resutling modelled ages. Varying the amphibolite-facies temperature and pressure conditions by ±50 °C and ±5 kbar, respesctively, leads

Table 3
A) Diffusion modelling results. Shown are the predicted model $^{40}Ar/^{39}Ar$ ages for phengite, biotite, and plagioclase for various cooling rates given various starting ages for the timing of peak metamorphism (U-Pb zircon) and amphibolite-facies cooling (U-Pb titanite). The modelled time difference between the start of the model and the resulting age (Δt) for each of the minerals is shown at varying cooling rates. B) Results of sensitivity testing showing the standard deviation of the model age output by varying the peak temperature and pressure (Peak T, Peak P) of the phengite models, and the temperature and pressure of the the amphbolite-facies conditions (Amp T, Amp P) for phengite, biotite, and plagioclase.

Table 3a

Modelled cooling of the Western Gneiss Region from zircon and titanite U-Pb age (Ma)

			Cooling rate (°CMa^{-1})				
			10	25	50	70	100
Phengite		Δt	29.6	11.1	5.2	3.6	2.5
		T_C	510	527	541	548	555
Oldest U—Pb zrn (Ma)	410		380	399	405	406	408
Mean U—Pb zrn (Ma)	405		375	394	400	401	403
Youngest U—Pb zrn (Ma)	400		370	389	395	396	398
Symplectite biotite		Δt	35.0	13.4	6.5	4.6	3.1
		T_C	324	338	348	353	359
Youngest U—Pb zrn (Ma)	400		365	387	394	395	397
Wtd Av U—Pb ttn (Ma)	393		358	380	387	388	390
Youngest U—Pb ttn (Ma)	379		344	366	373	374	376
Symplectite plagioclase		Δt	34.6	13.2	6.3	4.4	3.1
		T_C	325	340	352	358	364
Youngest U—Pb zrn (Ma)	400		365	387	394	396	397
Wtd Av U—Pb ttn (Ma)	393		358	380	387	389	390
Youngest U—Pb ttn (Ma)	379		344	366	373	375	376
Idioblastic biotite		Δt	32.9	12.5	6.0	4.2	2.9
		T_C	345	359	370	376	382
Youngest U—Pb zrn (Ma)	400		367	388	394	396	397
Wtd Av U—Pb ttn (Ma)	393		360	381	387	389	390
Youngest U—Pb ttn (Ma)	379		346	367	373	375	376

Table 3b

Sensitivity analysis results

		Phengite					Biotite		Plagioclase	
		Grain size	Peak T	Peak P	Amp T	Amp P	Grain size	Amp T	Grain size	Amp T
		0.25–1.5 mm	±50 °C	±1.5 kbar	±50 °C	±5 kbar[a]	0.25–1.5 mm	±50 °C	0.25–1.5 mm	±50 °C
Cooling rate (°CMa^{-1})	10	3.0	0.0	0.0	5.3	1.5	2.5	5.0	2.9	5.0
	25	1.3	0.0	0.0	2.1	0.6	1.1	2.0	1.2	2.0
	50	0.6	0.0	0.0	1.1	0.3	0.6	1.0	0.6	1.0
	70	0.5	0.0	0.0	0.8	0.3	0.4	0.8	0.5	0.8
	100	0.4	0.0	0.0	0.6	0.2	0.3	0.5	0.4	0.5

[a] Average.

to an uncertainy on the resutling model age of ±5.3–0.6 Ma and 1.5–0.2 Ma for cooling rates from 10°CMa^{-1} to 100°CMa^{-1} (Table 3b).

For biotite and plagioclase models, varying the model starting temperature by ±50 °C results in uncertainities on the model ages of 5.0–0.5 Ma for cooling rates from 10°CMa^{-1} to 100°CMa^{-1} for both minerals (Table 3b).

For all other parameters being equal, the variation between the modelled age of grains between 1.5 mm to 0.25 mm yields a ± 3.0–0.4 Ma uncertainty on the final age of the phengite models, ±2.5–0.3 Ma uncertainy on the biotite models, and a ±2.9–0.4 Ma uncertainty on the plagioclase models for cooling rates between 10°CMa^{-1} and 100°CMa^{-1} (Table 3b).

Dependent upon the bulk rock composition, titanite either crystallizes after the symplectite growth (as documented here), or may be contemporaneous with symplectite growth (Spencer et al., 2013). The reported U—Pb titanite ages for the Nordfjord area range from 399 to 379 Ma, with a weighted mean of 393 ± 4 Ma (Spencer et al., 2013). Since the diffusion models are calculated relative to the U—Pb titanite age, the 20 Ma spread in the titanite U—Pb data results in a 20 Ma spread in expected $^{40}Ar/^{39}Ar$ ages. Cooling may have begun prior to 393 Ma but the ±4 (2σ) uncertainties on the U—Pb and average ± 8 Ma (2σ) uncertainties on the $^{40}Ar/^{39}Ar$ ages means that any variation on the timing of amphibolite-facies crystallization is lost within the uncertainties of the datasets. Given the uncertainties in the U—Pb ages, diffusion model results, and the pseudosection calculations, we have taken the weighted mean of the U—Pb titanite ages (393 Ma) to represent the timing of cooling initiation for the purposes of this discussion.

Measured age ranges for phengite, symplectite biotite, symplectite plagioclase and idioblastic biotite are c.518–389 Ma, c.488–330 Ma, c.434–378 Ma, and c.449–377 Ma, respectively. These age ranges are much greater than the age range predicted by simple diffusion modelling despite uncertainties in the cooling rate and effective diffusive grain size (Fig. 6). The phengite $^{40}Ar/^{39}Ar$ ages are mostly older than those predicted by diffusion models, regardless of whether the weighted mean or the youngest age is compared with the model results. The phengite ages are also generally older than the reference titanite age, suggesting that phengite displays little diffusive resetting despite the high temperatures (700–750 °C). Overall the phengite $^{40}Ar/^{39}Ar$ ages are not therefore interpretable as cooling ages, a conclusion also reached by previous studies (McDonald et al., 2016; Warren et al., 2012a).

Biotite ages are consistently younger, with a smaller spread than phengite, though the ages are still overall older than expected from the diffusion models (Fig. 6). There is little consistent difference in age between the smaller, earlier-crystallized biotite in the symplectite and the larger, later, idioblastic grains, although the idioblastic grains yield a wider range but with overlapping errors. The similar ages yielded by biotites across a range of grain sizes either suggests that diffusive loss of Ar was inefficient, even at temperatures >680 °C (and therefore

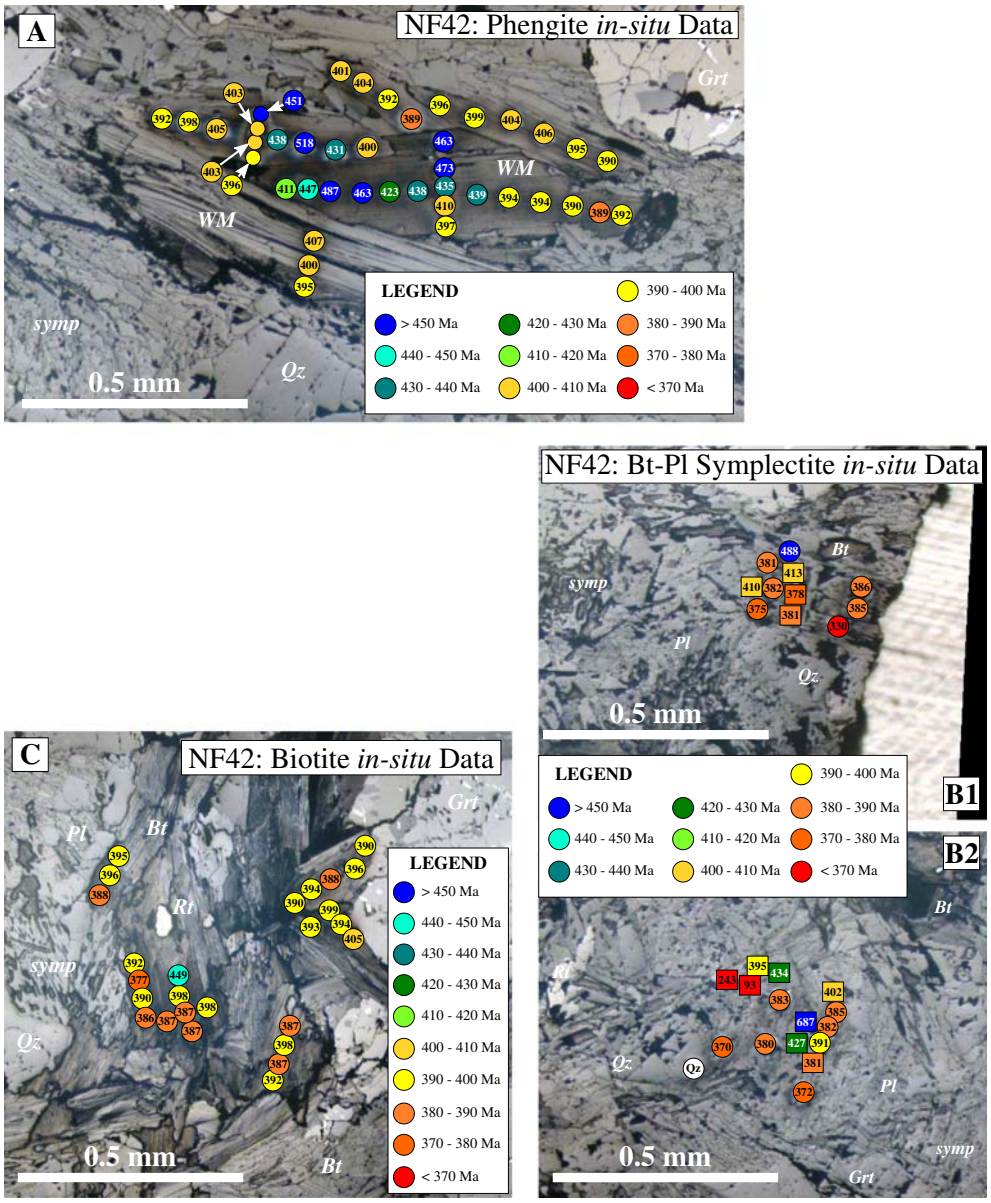

Fig. 5. Reflected-light photomicrographs of in-situ $^{40}Ar/^{39}Ar$ analyses. A) phengite showing a heterogeneous age distribution, with patchy "old" ages; B1) and B2) in-situ analysis of the symplectites produced from the breakdown of phengite. B1 shows analysis of symplectite that pseudomorphs the original phengite while B2, shows analysis from randomly orientated symplectite. Circles represent biotite analyses and squares, plagioclase; C) $^{40}Ar/^{39}Ar$ in-situ analysis of idioblastic biotite showing a more homogeneous age distribution.

that most of the ages cannot be considered true "Dodson" cooling ages), or that the rate of cooling experienced by this sample was fast enough to yield little difference between the biotite age of differing grain sizes.

The plagioclase ages also span a considerable range (434–378 Ma). The plagioclase has low K concentrations (average 0.1 wt%), and consequently some of the variability may be due to low measured ^{39}Ar concentrations and the presence of fluid inclusions. It is therefore plausible that the elevated plagioclase $^{40}Ar/^{39}Ar$ ages represent either crystal-lattice-hosted or fluid-inclusion-hosted contamination by excess ^{40}Ar.

Despite the uncertainty in the timing of initiation of cooling of the WGR, there is clearly a disparity between both the observed $^{40}Ar/^{39}Ar$ ages (and age ranges) and the modelled ages derived from DiffArg_P. Overall the data suggests that a diffusion model for Ar distribution that includes a fully open grain boundary network and a zero-concentration crystallization state is inadequate for the interpretation of the phengite, biotite, and plagioclase ages as cooling ages.

5. Implications: crystallization vs. contamination

As the $^{40}Ar/^{39}Ar$ phengite, biotite, and plagioclase ages measured in the WGR cannot be interpreted as simple thermally-activated diffusive loss in an open system, they may instead reflect either the timing of their crystallization, 'contamination' with excess ^{40}Ar, inefficient diffusive loss or a combination.

5.1. Phengite

The pseudosection in Fig. 4 and petrographic textures (Fig. 2A) indicate that phengite crystallized at $P < 25$ kbar and $T < 770$ °C. The timing of peak metamorphism has been constrained by U—Pb zircon at c. 410–400 Ma (Kylander-Clark and Hacker, 2014; Root et al., 2004; Young and Kylander-Clark, 2015). Therefore, if the $^{40}Ar/^{39}Ar$ phengite ages represent the timing of their crystallization, they should be similar. The model results suggest that to be consistent with open system

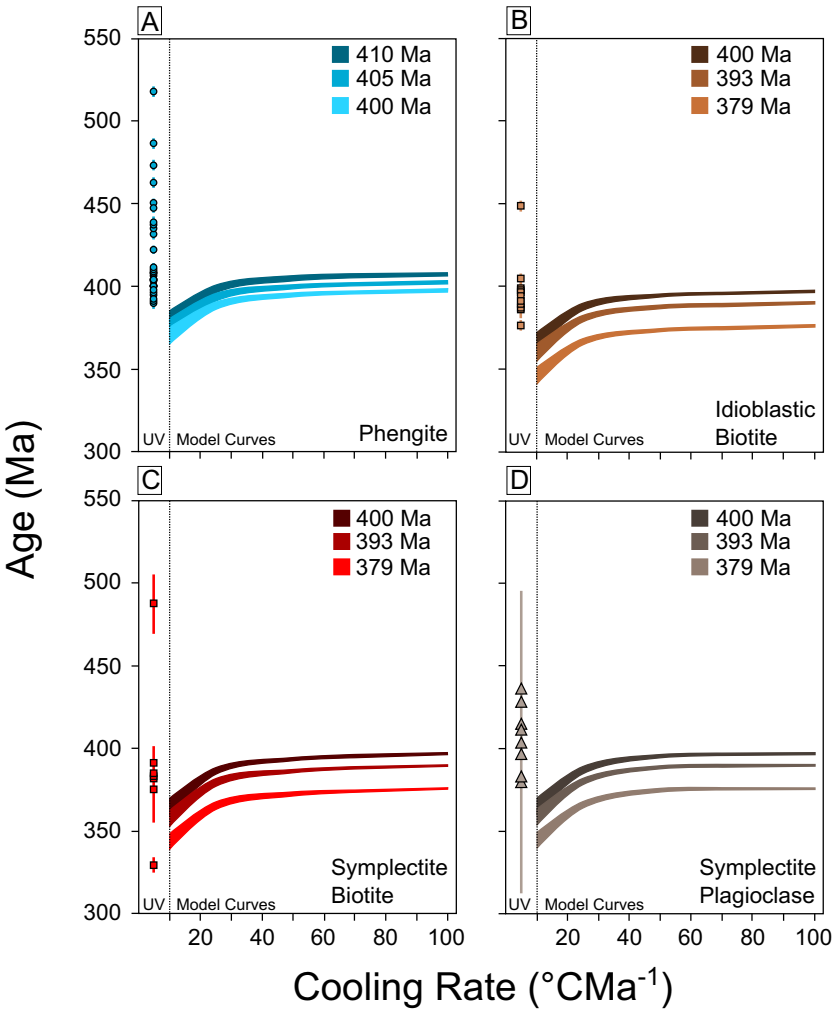

Fig. 6. A plot of the UV laser ablation data vs. the predicted modelled age curves for A) Phengite, B) idioblastic bioite, C) symplectite biotite, and D) symplectite plagioclase. The predicted model age curves are shown with their greatest uncertainty as defined by the sensitivity modelling in Table 3b.

cooling, the phengite ages should be 21–3 Ma younger than the timing of crystallization, depending upon the cooling rate.

The observed phengite $^{40}Ar/^{39}Ar$ ages span a range of c.518–389 Ma, far greater than the spread expected for crystallization ages. The ages between c. 400–389 Ma imply that these grains lost some ^{40}Ar, but not enough compared to the loss expected for a fully open system. The ages >410 Ma suggest contamination that occurred during decompression, with Ar having diffused into the phengite from either the grain boundary fluid, adjacent grains, or incorporated into the phengite crystal lattice during crystallization. The data do not allow these two scenarios to be separated. The 'old' ages within the phengite crystals are concentrated in patches that are not associated with the geographic cores of the grains. Chemical maps (Fig. 3A) do not indicate the presence of zoning within the grains. The contaminating ^{40}Ar may therefore be held within microstructural defects in the phengite.

5.2. Biotite

The pseudosection suggests that the biotite crystallized during near isothermal decompression at $P < 12$ kbar, T ~ 700 °C and pre-dates titanite formation. Therefore, the timing of biotite crystallization is constrained by the youngest U—Pb zircon age (400 Ma) and the weighted mean titanite age (393 Ma).

The symplectite biotite ages lie between c.488–330 Ma, a greater-than-expected spread given the grain size variation for a fixed regional cooling rate (Fig. 6). The larger idioblastic biotites range in age from c. 449–377 Ma; which is also greater than that predicted from simple open system cooling models (Fig. 6). Furthermore, the symplectite biotite is texturally older than the idioblastic biotite, yet yields ages that are less dispersed but lie within the same range. We therefore suggest that the idioblastic biotite ages show patchy evidence for ^{40}Ar contamination. This contamination mostly likely occurred during crystallization and growth, but may also have occurred during exhumation and cooling.

5.3. Plagioclase

Evidence for the presence of fluid that is enriched in ^{40}Ar comes from the dates yielded by the plagioclase that co-crystallized with the biotite during symplectization of HP phengite. The plagioclase yields very scattered and generally "old" ages that are considerably older than the ages yielded by the co-crystallizing biotite (Fig. 6). The source of the contaminating ^{40}Ar was most probably the reacting phengite. The 'excess' ^{40}Ar measured in the plagioclase implies that the grain boundary network was poorly interconnected, at least on the local scale.

6. Conclusions

Textural evidence for the reactions between different K-bearing minerals within the same sample combined with spatially-detailed in-situ $^{40}Ar/^{39}Ar$ analyses can offer insights into how efficiently Ar is removed or recycled during high temperature metamorphism. In the WGR, gneisses that reached eclogite facies (~20–25 kbar) conditions

at c. 410–400 Ma followed by isothermal decompression to <12 kbar, record mineralogical evidence for all these stages. In-situ laser ablation $^{40}Ar/^{39}Ar$ data from phengite and the biotite–plagioclase symplectites that replace it yield wide age ranges that help to constrain how Ar behaves during recrystallization.

Phengite which grew at 20–25 kbar and 670–770 °C and which subsequently partially broke down during decompression yields ages ranging from 518 to 389 Ma. Heterogeneous Ar distributions within and between grains suggest little diffusive resetting despite the high temperatures experienced after crystallization. Ages older than the estimated timing of crystallization suggest ^{40}Ar contamination during crystallization or decompression.

Symplectites that grew from phengite during decompression at $P < 12$ kbar document the partial redistribution of phengite-hosted Ar. $^{40}Ar/^{39}Ar$ ages of symplectite biotite grains that are "older" than those predicted from diffusion modelling suggest that either they incorporated Ar during their growth, or that they degassed inefficiently. The plagioclase that co-crystallized with the symplectite biotite yields ages that reflect contamination and incorporation of ^{40}Ar, possibly in fluid inclusions and not related to K in the plagioclse lattice. These data point towards plagioclase acting as a sink for the ^{40}Ar released by phengite during breakdown. $^{40}Ar/^{39}Ar$ ages of idioblastic biotite that grew at <12 kbar, show that as biotite coarsened following initial crystallization, Ar released during the breakdown of phengite was still present in the rock volume and that the grain boundary network within the rock was partially closed to Ar loss. These lines of evidence combine to indicate that the grain boundary network was partially closed during exhumation and symplectite-formation.

None of the measured ages can be reconciled with models of simple thermally-activated diffusion during cooling in a purely open system. Instead the ages of the phengite reflect contamination (which may have occurred during either crystallization or along the decompression path) and inefficient Ar loss. The plagioclase and biotite ages reflect continuing contamination by Ar released during the breakdown of phengite, within a grain boundary network with very restricted advection of either Ar or hydrous fluids.

Overall, these data demonstrate that even at high temperature metamorphic conditions, Ar may not diffuse efficiently out of micas unless there is sufficient advection of the grain boundary fluids. These datasets show that $^{40}Ar/^{39}Ar$ ages, and their interpretation may vary from sample to sample and mineral to mineral, even in the same terrain. The petrographic evolution of each rock should be carefully documented in order to provide a (relative) temporal framework in which to interpret the $^{40}Ar/^{39}Ar$ data. Furthermore, the analysis of multiple minerals aids the determination of how Ar has behaved during metamorphic recrystallization. Overall this approach allows ^{40}Ar mobility and distribution to be more precisely linked to a samples metamorphic evolution.

Supplementary data to this article can be found online at https://doi.org/10.1016/j.lithos.2017.11.028.

Acknowledgements

CSM was funded on an Open University Charter Studentship. DR acknowledges financial support from an SNF Fellowship (PBBEP2_142167). CJW acknowledges financial support from a NERC Advanced Fellowship (NE/H016279/1) and a NERC small grant (NE/J013072/1). Laboratory and technical assistance from Alison Halton, Michelle Higgins, Sam Hammond, and James Malley was gratefully received. An anonymous reviewer is thanked for insightful comments that improved the manuscript.

References

Allaz, J., Engi, M., Berger, A., Villa, I.M., 2011. The effects of retrograde reactions and of diffusion on $^{40}Ar/^{39}Ar$ ages of micas. Journal of Petrology 52:691–716. https://doi.org/10.1093/petrology/egq100.

Anderson, E.D., Moecher, D.P., 2007. Ompacite breakdown reactions and relation to eclogite exhumation rates. Contributions to Mineralogy and Petrology 154: 253–277. https://doi.org/10.1007/s00410-007-0192-x.

Anderson, J.L., Smith, D.R., 1995. The effect of temperature and oxygen fugacity on al-in-hornblende barometry. American Mineralogist 80:549–559. https://doi.org/10.2138/am-1995-5-614.

Baxter, E.F., DePaolo, D.J., Renne, P.R., 2002. Spatially correlated anomalous $^{40}Ar/^{39}Ar$ "age" variations in biotites about a lithologic contact near Simplon pass, Switzerland: a mechanistic explanation for excess Ar. Geochimica et Cosmochimica Acta 66:1067–1073. https://doi.org/10.1016/S0016-7037(01)00828-6.

Beltrando, M., Di Vincenzo, G., Ferraris, C., 2013. Preservation of sub-microscopic structural relicts in micas from the gran Paradiso massif (western alps): implications for $^{40}Ar/^{39}Ar$ geochronology. Geochimica et Cosmochimica Acta 119:359–380. https://doi.org/10.1016/j.gca.2013.05.043.

Berry, H.N., Lux, D.R., Andresen, A., Andersen, T.B., 1995. Progressive exhumation during orogenic collapse as indicated by $^{40}Ar/^{39}Ar$ cooling ages from different structural levels, southwest Norway. Geolognytt 22, 20–21.

Blundy, J.D., Holland, T.J.B., 1990. Calcic amphibole equilibria and a new amphibole-plagioclase geothermometer. Contributions to Mineralogy and Petrology 104: 208–224. https://doi.org/10.1007/BF00306444.

Bryhni, I., 1966. Reconnaissance studies of gneisses, ultrabasites, eclogites and anorthosites in outer Nordfjord, western Norway. Norges Geologiske Undersøkelse 241, 1–68.

Connolly, J.A.D., 1990. Multivariable phase diagrams: an algorithm based on generalized thermodynamics. American Mineralogist 290:666–718. https://doi.org/10.2475/ajs.290.6.666.

Cuthbert, S.J., Carswell, D.A., Krogh-Ravna, E.J., Wain, A., 2000. Eclogites and eclogites in the western gneiss region, Norwegian Caledonides. Lithos 52:165–195. https://doi.org/10.1016/S0024-4937(99)00090-0.

Dale, J., Holland, T., Powell, R., 2000. Hornblende – garnet – plagioclase thermobarometry: a natural assemblage calibration of the thermodynamics of hornblende. Contributions to Mineralogy and Petrology 140:353–362. https://doi.org/10.1007/s004100000187.

de Sigoyer, J., Chavagnac, V., Blichert-Toft, J., Villa, I.M., Luais, B., Cosca, M.A., Mascle, G., 2000. Dating the Indian continental subduction and collisional thickening in the northwest Himalaya: multichronology of the Tso Morarieclogites. Geology 28: 487–490. https://doi.org/10.1130/0091-7613(2001)029<0192:R>2.0.CO;2.

Di Vincenzo, G., 2006. Comparison of $^{40}Ar/^{39}Ar$ and Rb-Sr data on phengites from the UHP Brossasco-Isasca unit (Dora Maira Massif, Italy): implications for dating white mica. Journal of Petrology 47:1439–1465. https://doi.org/10.1093/petrology/egl018.

Dodson, M.H., 1973. Closure temperature in cooling geochronological and petrological systems. Contributions to Mineralogy and Petrology 40:259–274. https://doi.org/10.1007/BF00373790.

Dransfield, M., 1994. Extensional Exhumation of High-Grade Rocks in Western Norway and the Zanskar Himalaya. University of Oxford.

Engvik, A., Andersen, T., Wachmann, M., 2007. Inhomogeneous deformation in deeply buried continental crust, an example from the eclogite-facies province of the western gneiss region, Norway. Norges Geologisk Tidsskrift 87, 373–389.

Eskola, P., 1921. On the eclogites of Norway. Norske vidsenskaps-akademi i Oslo. Matematisk-naturvidenskabelig klasse 8 (118 pp).

Frost, B.R., Chamberlain, K.R., Schumacher, J.C., 2001. Sphene (titanite): phase relations and role as a geochronometer. Chemical Geology 172:131–148. https://doi.org/10.1016/S0009-2541(00)00240-0.

Fuhrman, M.L., Lindsley, D.H., 1988. Ternary-feldspar modelling and thermometry. American Mineralogist 73, 201–215.

Gee, D., 1975. A tectonic model for the central part of the Scandinavian Caledonides. American Journal of Science 275, 468–515.

Gilotti, J.A., Krogh-Ravna, E.J., 2002. First evidence for ultrahighh-pressure metamorphism in the north-East Greenland Caledonides. Geology 30:551–554. https://doi.org/10.1130/0091-7613(2002)030<0551:FEFUPM>2.0.CO;2.

Godard, G., Mabit, J.-L., 1998. Peraluminoussapphirine formed during retrogression of a kyanite-bearing eclogite from Pay de Leon, Armorican Massif, France. Lithos 43: 15–29. https://doi.org/10.1016/S0024-4937(98)00004-8.

Groppo, C., Rolfo, F., Liu, Y.-C., Deng, L.-P., Wang, A.-D., 2015. P-T evolution of elusive UHP eclogites from the Luotian dome (north Dabie zone, China): how far can the thermodynamic modeling lead us? Lithos 226:183–200. https://doi.org/10.1016/j.lithos.2014.11.013.

Hacker, B.R., 2007. Ascent of the ultrahigh-pressure western gneiss region, Norway. Geological Society of America Special Papers 419:171–184. https://doi.org/10.1130/2006.2419(09).

Hacker, B.R., Gans, P.B., 2005. Continental collisions and the creation of ultrahigh-pressure terranes: petrology and thermochronology of nappes in the central Scandinavian Caledonides. Geological Society of America Bulletin 117:117–134. https://doi.org/10.1130/B25549.1.

Hacker, B.R., Calvert, A., Zhang, R.Y., Ernst, W.G., Liou, J.G., 2003. Ultrarapid exhumation of ultrahigh-pressure diamond-bearing metasedimentary rocks of the Kokchetav massif, Kazakhstan? Lithos 70:61–75. https://doi.org/10.1016/S0024-4937(03)00092-6.

Hacker, B.R., Andersen, T.B., Johnston, S., Kylander-Clark, A.R.C., Peterman, E.M., Walsh, E.O., Young, D.J., 2010. High-temperature deformation during continental-margin subduction & exhumation: the ultrahigh-pressure Western Gneiss Region of Norway. Tectonophysics 480:149–171. https://doi.org/10.1016/j.tecto.2009.08.012.

Heinrich, C., 1982. Kyanite-eclogite to amphibolite facies evolution of hydrous mafic and pelitic rocks, Adula nappe, central alps. Contributions to Mineralogy and Petrology 81:30–38. https://doi.org/10.1007/BF00371156.

Holland, T., Blundy, J., 1994. Non-ideal interactions in calcic amphiboles and their bearing on amphibole-plagioclase thermometry. Contributions to Mineralogy and Petrology 116:433–447. https://doi.org/10.1007/BF00310910.

Holland, T.J.B., Powell, R., 1996. Thermodymanics of order-disorder in minerals. 2. Symmetric formulism applied to solid solutions. American Mineralogist 81, 1425–1437 (doi: 0003-004X/96/l112-1425).
Holland, T.J.B., Powell, R., 1998. An internally consistent thermodynamic data set for phases of petrological interest. Journal of Metamorphic Geology 16:309–343. https://doi.org/10.1111/j.1525-1314.1998.00140.x.
Holland, T., Powell, R., 2001. Calculations of phase relations involving haplogranitic melts using internally consistent thermodynamic dataset. Journal of Petrology 42:673–683. https://doi.org/10.1093/petrology/42.4.673.
Holland, T.J.B., Powell, R., 2011. An improved and extended internally consistent thermodynamic dataset for phases of petrological interest, involving a new equation of state for solids. Journal of Metamorphic Geology 29:333–383. https://doi.org/10.1111/j.1525-1314.2010.00923.x.
Holland, T.J.B., Baker, J., Powell, R., 1998. Mixing properties and activity-composition relationships of chlorites in the system MgO-FeO-Al_2O_3-SiO_2-H_2O. European Journal of Mineralogy 10, 395–406 (doi: 0935-1221/98/0010-0395).
Johnson, S.M., Hacker, B.R., Andersen, T.B., 2007. Exhuming Norwegian ultrahigh-pressure extensional structures and the role of the Nordfjord-Sogn detachment zone. Tectonics 26, TC5001. https://doi.org/10.1029/2005TC001933.
Kellett, D.A., Warren, C., Larsen, K.P., Zwingman, H., van Staal, C.R., Rogers, N., 2016. Influence of deformation and fluids on Ar retention in white mica: dating the dover fault, Newfoundland Appalachians. Lithos 254-255:1–17. https://doi.org/10.1016/j.lithos.2016.03.003.
Krogh, T.E., Kamo, S.L., Robinson, P., Terry, M.P., Kwok, K., 2011. U-Pb zircon geochronology of eclogites from the Scandian orogeny, northern western gneiss region, Norway: 14-20 million years between eclogite crystallization and return to amphibolite-facies conditions. Canadian Journal of Geoscience 48:441–472. https://doi.org/10.1139/e10-076.
Kylander-Clark, A.R.C., Hacker, B.R., 2014. Age and significance of felsic dykes from the UHP western gneiss region. Tectonics 33:2342–2360. https://doi.org/10.1002/2014TC003582.
Kylander-Clark, A.R.C., Hacker, B.R., Mattinson, J.M., 2008. Slow exhumation of UHP terranes: Titanite and rutile ages of the western gneiss region, Norway. Earth and Planetary Science Letters 272:531–540. https://doi.org/10.1016/j.epsl.2008.05.019.
Labrousse, L., Jolivet, L., Andersen, T.B., Agard, P., Hebert, R., Maluski, H., Scharer, U., 2004. Pressure–temperature-time-deformation history of the exhumation of ultra-high pressure rocks in the western gneiss region, Norway. Geological Society of America Special Papers 380:155–185. https://doi.org/10.1130/0-8137-2380-9.155.
Li, S., Wang, S., Chen, Y., Liu, D., Qiu, J., Zhou, H., Zhang, Z., 1994. Excess argon in phengites from eclogites: evidence from dating eclogite minerals by Sm-Nd, Rb-Sr and $^{40}Ar/^{39}Ar$ methods. Chemical Geology 112:343–350. https://doi.org/10.1016/0009-2541(94)90033-7.
Li, S., Jagoutz, E., Lo, C.-H., Chen, Y., Li, Q., Xiao, Y., 1999. Sm/Nd, Rb/Sr, and $^{40}Ar/^{39}Ar$ isotopic systematics of the ultrahigh-pressure metamorphic rocks in the Dabie-Sulu Belt, Central China: a retrospective view. International Geology Review 41:1114–1124. https://doi.org/10.1080/00206819909465195.
Lux, D.R., 1985. K/Ar ages from the basel gneiss region, Stadlandet area, western Norway. Norsk Geologisk Tidsskrift 65, 277–286.
McDonald, C.S., Warren, C.J., Mark, D.F., Halton, A.M., Kelley, S.P., Sherlock, S.C., 2016. Argon redistribution during a metamorphic cycle: consequences for determining cooling rates. Chemical Geology 443:182–197. https://doi.org/10.1016/j.chemgeo.2016.09.028.
Mulch, A., Cosca, M.A., 2004. Recystallization or cooling ages: in situ UV-laser $^{40}Ar/^{39}Ar$ geochronology of muscovite in mylonitic rocks. Journal of the Geological Society of London 161:573–582. https://doi.org/10.1144/0016-764903-110.
Peterman, E.M., Hacker, B.R., Baxter, E.F., 2009. Phase transformations of continental crust during subduction and exhumation: western gneiss region, Norway. European Journal of Mineralogy 21:1097–1118. https://doi.org/10.1127/0935-1221/2009/0021-1988.
Putlitz, B., Cosca, M.A., Schumacher, J.C., 2005. Prograde mica $^{40}Ar/^{39}Ar$ growth ages recorded in high pressure rocks (Syros, Cyclades, Greece). Chemical Geology 214:79–98. https://doi.org/10.1016/j.chemgeo.2004.08.056.
Renne, P.R., Balco, G., Ludwig, K.R., Mundil, R., Min, K., 2011. Response to the comment by Schwarz et al., on joint determination of ^{40}K decay constants and $^{40}Ar^*/^{40}K$ for the fish canyon sanidine standard, and improved accuracy for $^{40}Ar/^{39}Ar$ geochronology by P.R. Renne et al. (2010). Geochimica et Cosmochimica Acta 75:5097–5100. https://doi.org/10.1016/j.gca.2011.06.021.
Roberts, D., 2003. The Scandinavian Caledonides: event chronology, paleogeographic settings and likely modern analogues. Tectonophysics 365:283–299. https://doi.org/10.1016/S0040-1951(03)00026-X.
Root, D.B., Hacker, B.R., Mattinson, J.M., Wooden, J.L., 2004. Zircon geochronology and ca. 400 Ma exhumation of Norwegian ultrahigh-pressure rocks: an ion microprobe and chemical abrasion study. Earth and Planetary Science Letters 228:325–341. https://doi.org/10.1016/j.epsl.2004.10.019.
Root, D.B., Hacker, B.R., Gans, P.B., Ducea, M.N., Eide, E.A., Mosenfelder, J.L., 2005. Discrete ultrahigh-pressure domains in the western gneiss region, Norway: implications for formation and exhumation. Journal of Metamorphic Geology 23:45–61. https://doi.org/10.1111/j.1525-1314.2005.00561.x.
Schärer, U., Labrousse, L., 2003. Dating the exhumation of UHP rocks and associated crustal melting in the Norwegian Caledonides. Contributions to Mineralogy and Petrology 144:758–770. https://doi.org/10.1007/s00410-002-0428-8.
Schmidt, M.W., 1992. Amphibole composition in tonalite as a function of pressure: an experimental calibration of the al-in-hornblende barometer. Contributions to Mineralogy and Petrology 110:304–310. https://doi.org/10.1007/BF00310745.
Sherlock, S.C., Kelley, S., 2002. Excess argon evolution in HP-LT rocks: a UVLAMP study of phengite and K-free minerals, NW Turkey. Chemical Geology 182:619–636. https://doi.org/10.1016/S0009-2541(01)00345-X.
Smith, D., 1984. Coesite in clinopyroxene in the Caledonides and its implications for geodynamics. Nature 310:641–644. https://doi.org/10.1038/310641a0.
Spencer, K.J., Hacker, B.R., Kylander-Clark, A.R.C., Andersen, T.B., Cottle, J.M., Stearns, M.A., Poletti, J.E., Seward, G.G.E., 2013. Campaign-style titanite U–Pb dating by laser-ablation ICP: implications for crustal flow, phase transformations and titanite closure. Chemical Geology 341:84–101. https://doi.org/10.1016/j.chemgeo.2012.11.012.
Tajcmanová, L., Connolly, J.A.D., Cesare, B., 2009. A thermodynamic model for titanium and ferric iron solution in biotite. Journal of Metamorphic Geology 27:153–164. https://doi.org/10.1111/j.1525-1314.2009.00812.x.
Terry, M.P., Robinson, P., 2003. Evolution of amphibolite-facies structural features and boundary conditions for deformation during exhumation of high- and ultrahigh pressure rocks, Nordøyane, western gneiss region, Norway. Tectonics 22:1036. https://doi.org/10.1029/2001TC001349.
Terry, M.P., Robinson, P., Ravna, E.J.K., 2000. Kyanite eclogite thermobarometry and evidence for thrusting of UHP over HP metamorphic rocks, Nordøyane, western gneiss region, Norway. American Mineralogist 85, 1637–1650 (doi:).
Tucker, R.D., Råheim, A., Krogh, T.E., Corfu, F., 1987. Uranium-lead zircon and titanite ages from the northern portion of the western gneiss region, south-central Norway. Earth and Planetary Science Letters 81:203–211. https://doi.org/10.1016/0012-821X(87)90156-7.
Villa, I.M., 1997. Isotopic closure. Terra Nova 10:42–47. https://doi.org/10.1046/j.1365-3121.1998.00156.x.
Villa, I.M., Bucher, S., Bousquet, R., Kleinhanns, I.C., Schmid, S.M., 2014. Dating polygenetic metamorphic assemblages along a transect across the western alps. Journal of Petrology 55:803–830. https://doi.org/10.1093/petrology/egu007.
Wain, A., 1997. New evidence for coesite in eclogite and gneiss: defining an ultrahigh-pressure province in the western gneiss region, Norway. Geology 25:927–930. https://doi.org/10.1130/0091-7613(1997)025<0927:NEFCIE>2.3.CO;2.
Wain, A., Waters, D.J., Jephcoat, A., Olijynk, H., 2000. The high-pressure to ultrahigh-pressure eclogite transition in the western gneiss region, Norway. European Journal of Mineralogy 12:667–687. https://doi.org/10.1127/0935-1221/2000/0012-0667.
Walsh, E.O., Hacker, B.R., 2004. The fate of subducted continental margins: two-stage exhumation of the high-pressure to ultrahigh-pressure western gneiss complex, Norway. Journal of Metamorphic Geology 22:671–689. https://doi.org/10.1111/j.1525-1314.2004.00541.x.
Walsh, E.O., Hacker, B.R., Gans, P.B., Grove, M., Gehrels, G., 2007. Protolith ages and exhumation histories of (ultra)high-pressure rocks across the western gneiss region, Norway. Geological Society of America Bulletin 119:289–301. https://doi.org/10.1130/B25817.1.
Walsh, E.O., Hacker, B.R., Gans, P.B., Wong, M.S., Andersen, T.B., 2013. Crustal exhumation of the Western Gneiss Region UHP terrane, Norway: $^{40}Ar/^{39}Ar$ thermochronology and fault-slip analysis. Tectonophysics 608:1159–1179. https://doi.org/10.1016/j.tecto.2013.06.030.
Warren, C.J., Sherlock, S.C., Kelley, S.P., 2011. Interpreting high-pressure phengite $^{40}Ar/^{39}Ar$ laserprobe ages: an example from Saih Hatat, NE Oman. Contributions to Mineralogy and Petrology 161:991–1009. https://doi.org/10.1007/s00410-010-0576-1.
Warren, C.J., Hanke, F., Kelley, S.P., 2012a. When can muscovite $^{40}Ar/^{39}Ar$ dating constrain the timing of metamorphic exhumation? Chemical Geology 291:79–86. https://doi.org/10.1016/j.chemgeo.2011.09.017.
Warren, C.J., Kelley, S.P., Sherlock, S.C., McDonald, C.S., 2012b. Metamorphic rocks seek meaningful cooling rate: interpreting $^{40}Ar/^{39}Ar$ ages in an exhumed ultra-high pressure terrane. Lithos 155:30–48. https://doi.org/10.1016/j.lithos.2012.08.011.
Watson, J.S., 1996. Fast, simple method of powder pellet preparation for X-ray fluorescence analysis. X-Ray Spectrometry 25:173–174. https://doi.org/10.1002/(SICI)1097-4539(199607)25:4<173::AID-XRS158>3.0.CO;2-Z.
Wheeler, J., 1996. Diffarg: a program for simulating argon diffusion profiles in minerals. Computers & Geosciences 22:919–929. https://doi.org/10.1016/S0098-3004(96)00061-1.
White, R.W., Powell, R., Holland, T.J.B., Worley, B.A., 2000. The effect of TiO_2 and Fe_2O_3 on metapelitic assemblages at greenschist and amphibolite facies conditions: mineral equilibria calculations in the system K_2O-FeO-MgO-Al_2O_3-SiO_2-H_2O-TiO_2-Fe_2O_3. Journal of Metamorphic Geology 18:497–511. https://doi.org/10.1046/j.1525-1314.2000.00269.x.
White, R.W., Powell, R., Holland, T.J.B., 2001. Calculation of partial melting equilibria in the system Na_2O-CaO-K_2O-FeO-MgO-Al_2O_3-SiO_2-H_2O (NCKFMASH). Journal of Metamorphic Geology 19:139–153. https://doi.org/10.1046/j.0263-4929.2000.00303.x.
Whitney, D.L., Evans, B.W., 2010. Abbreviations for names of rock-forming minerals. American Mineralogist 95:185–187. https://doi.org/10.2138/am.2010.3371.
Young, D.J., Kylander-Clark, A.R.C., 2015. Does continental crust transform during eclogite facies metamorphism? Journal of Metamorphic Geology 33, 331–357.
Young, D.J., Hacker, B.R., Andersen, T.B., Corfu, F., 2007. Prograde amphibolite facies to ultrahigh-pressure transition along Nordfjord, western Norway: implications for exhumation tectonics. Tectonics 26, TC1007. https://doi.org/10.1029/2004TC001781.
Young, D., Hacker, B.R., Andersen, T.B., Gans, P.B., 2011. Structure and $^{40}Ar/^{39}Ar$ thermochronolgy of an ultrahigh-pressure transition in western Norway. Journal of the Geological Society of London 168:887–898. https://doi.org/10.1144/0016-76492010-075.